Hydrol. Earth Syst. Sci. Discuss., 6, 6425–6454, 2009
www.hydrol-earth-syst-sci-discuss.net/6/6425/2009/

Hydrology and Earth System Sciences Discussions

Papers published in *Hydrology and Earth System Sciences Discussions* are under open-access review for the journal *Hydrology and Earth System Sciences*

Relating surface backscatter response from TRMM Precipitation Radar to soil moisture: results over a semi-arid region

H. Stephen[1], **S. Ahmad**[1], **T. C. Piechota**[1], **and C. Tang**[2]

[1]Department of Civil and Environmental Engineering, University of Nevada, Las Vegas, NV 89154, USA
[2]Department of Geosciences, Idaho State University, Pocatello, ID 83209, USA

Received: 5 October 2009 – Accepted: 8 October 2009 – Published: 22 October 2009

Correspondence to: S. Ahmad (sajjad.ahmad@unlv.edu)

Published by Copernicus Publications on behalf of the European Geosciences Union.

Abstract

The Tropical Rainfall Measuring Mission (TRMM) carries aboard the Precipitation Radar (TRMMPR) that measures the backscatter (σ°) of the surface. σ° is sensitive to surface soil moisture and vegetation conditions. Due to sparse vegetation in arid and semi-arid regions, TRMMPR σ° primarily depends on the soil water content. In this study we relate TRMMPR σ° measurements to soil water content (m_s) in Lower Colorado River Basin (LCRB). σ° dependence on m_s is studied for different vegetation greenness values determined through Normalized Difference Vegetation Index (NDVI). A new model of σ° that couples incidence angle, m_s, and NDVI is used to derive parameters and retrieve soil water content. The calibration and validation of this model are performed using simulated and measured m_s data. Simulated m_s is estimated using Variable Infiltration Capacity (VIC) model whereas measured m_s is acquired from ground measuring stations in Walnut Gulch Experimental Watershed (WGEW).

σ° model is calibrated using VIC and WGEW m_s data during 1998 and the calibrated model is used to derive m_s during later years. The temporal trends of derived m_s are consistent with VIC and WGEW m_s data with correlation coefficient (R) of 0.89 and 0.74, respectively. Derived m_s is also consistent with the measured precipitation data with R=0.76. The gridded VIC data is used to calibrate the model at each grid point in LCRB and spatial maps of the model parameters are prepared. The model parameters are spatially coherent with the general regional topography in LCRB. TRMMPR σ° derived soil moisture maps during May (dry) and August (wet) 1999 are spatially similar to VIC estimates with correlation 0.67 and 0.76, respectively. This research provides new insights into Ku-band σ° dependence on soil water content in the arid regions.

1 Introduction

The ongoing drought of the Colorado River Basin in the South Western United States started in 2000 and has become the longest drought in the recorded history of the

HESSD

6, 6425–6454, 2009

basin. This is evident from the historic low levels in most of the storage lakes that has resulted in severe water shortage in some user states. Colorado River Basin provides water to seven states in the US and a part of Mexico. Due to the regional importance of this basin and agricultural and social impacts of water scarcity, it is important to understand the factors related to droughts. Timely information of possible drought can improve decisions for water management. Drought signatures are closely related to the spatial and temporal variability of soil moisture. Soil water content reflects the recent precipitation, agricultural potential, and water storage and can serve as a good index of drought (Sheffield et al., 2004; Cosh et al., 2008).

Soil moisture is an important variable for understanding the hydrology and climate. It is an integral part of water and energy balance equations in atmospheric and hydrologic models. Microwave remote sensing with its sensitivity to dielectric properties is useful in mapping the land surface soil moisture (Schmugge, 1983; Behari, 2005; Pulliainen et al., 1998; Baup et al., 2007). Its dependence on spatial and temporal variability of surface dielectric constant is useful to monitor soil moisture at basin scales. Recent research directions indicate rising interest in the operational measuring and monitoring of the global soil moisture using remote sensing (Njoku et al., 2003; Moran et al., 2004; Wagner et al., 2007). National Aeronautics and Space Administration plans to launch a dedicated soil moisture mapping mission called Soil Moisture Active Passive (SMAP) in 2012 (Barrett et al., 2009). Similar mission called Soil Moisture and Ocean Salinity (SMOS) is to be launched by European Space Agency in 2009 (ESA Study Report, 2004). Thus, it is important to further expand the hydrological applications of the microwave remote sensing data.

Microwave backscatter (σ°) depends on soil moisture and vegetation conditions of land surface. Decoupling the effects of soil and vegetation on backscatter poses a major difficulty for useful application (Magagi and Kerr, 1997; Woodhouse and Hoekman, 2000). The presence of vegetation reduces σ° sensitivity to soil moisture. Vegetation is sparse in arid and semi-arid regions and thus, backscatter measurements in such areas primarily depend on the soil moisture and soil roughness characteristics. Vari-

HESSD
6, 6425–6454, 2009

ous theoretical and empirical models have been devised to retrieve soil moisture from active and passive remote sensing data (Ulaby et al., 1982; Fung, 1994; Wen et al., 2003; Bindlish et al., 2003; Paloscia et al., 2001). Theoretical models involve complicated scattering phenomena from probabilistic models of soil, vegetation, and terrain. They model plant leaves as thin disks, branches and trunks as cylinders, and soil surface by the standard deviation and correlation length of surface height (Shi et al., 1997; Rahman et al., 2008). Generally, such models are computationally intensive and difficult to implement in large scale applications. Empirical models of backscatter (σ°) are data driven and can be implemented with relative ease given sufficient in-situ data for calibration and validation. The purpose of this study is to investigate and model σ° incidence angle (θ) response and develop a model for soil moisture retrieval. In-situ soil moisture data is not widely available and is sparse for regional scale modeling. Soil moisture experiments (SMEX) have considerably helped in the development of remote sensing of soil moisture but the soil moisture measurements from these experiments are only available for a few selected locations (Das et al., 2008). Simulated soil moisture spatial maps from the basin scale hydrological models can fill this gap for the purposes of calibration and validation.

Generally, backscatter at C- and L-bands has better sensitivity to soil moisture than Ku-band due to relatively lesser attenuation by vegetation stand (Ulaby et al., 1982). Future missions of SMAP and SMOS operating in L-band would provide data with better sensitivity to soil moisture. Meanwhile, over arid regions with low vegetation, it would be beneficial to understand σ° and its θ-response in relation to soil moisture at basin scale.

The Tropical Rainfall Measuring Mission (TRMM) Precipitation Radar (TRMMPR), initially designed to measure rainfall (Kummerow et al., 1998; Kozu et al., 2001), provides Ku-band HH polarization σ° measurements of the land surface. Earlier studies on TRMMPR σ° have shown it to be sensitive to the surface soil moisture (Seto et al., 2003; Narayan et al., 2006), but no comprehensive method has been developed for a systematic retrieval of soil moisture spatial maps from TRMMPR Ku-band data. Gen-

HESSD
6, 6425–6454, 2009

erally, Ku-band radiation is attenuated by the vegetation canopy but in the arid regions, due to sparse and shrubland-like vegetation, it has primary dependence on soil characteristics.

In this paper, TRMMPR Ku-band σ° dependence on soil water content (m_s) is investigated in the arid region of Lower Colorado River Basin (LCRB). Backscatter, in decibels (dB), is modeled as a function of θ, m_s, and Normalized Difference Vegetation Index (NDVI); and calibrated using known soil moisture data. σ° model is calibrated using 1998 data and used to derive m_s during later years. Known data consists of simulated soil moisture data from hydrologic modeling and measured data from ground stations. Simulated m_s is estimated for top 10 cm soil layer by Variable Infiltration Capacity (VIC) model (Liang et al., 1994; Tang, 2007) whereas measured m_s is acquired for top 5 cm soil layer at ground measuring stations in Walnut Gulch Experimental Watershed (WGEW). Soil moisture derived from σ° model is validated using in-situ measurements and climate division monthly average precipitation data. The results show the potential of Ku-band instruments over arid and semi-arid regions.

This paper is organized as follows. Section 2 describes the study area and characteristics of the data used in this research. This is followed by the description of research approach and methods in Sect. 3. σ° model, model parameters, and model calibration are also discussed in this section. Section 4 presents the results and discussion. The model derived soil moisture and its comparison with the time series of measured soil moisture and precipitation data is also presented. The spatial distribution of soil moisture in LCRB is derived and compared to the VIC m_s estimates. Finally, in Sect. 5 conclusions are presented.

2 Study area and data

This section describes the characteristics of the study area and the data used in this investigation. The TRMMPR sensor specifications and NDVI data characteristics are provided. VIC model development to produce simulated soil moisture is also described.

HESSD
6, 6425–6454, 2009

2.1 Colorado River Basin

Colorado River Basin provides water supply, flood control, and hydropower to a large area of the southwest United States. The basin drains an area of 637 000 square kilometers (246 000 square miles), including parts of seven western US states, Wyoming, Colorado, Utah, New Mexico, Nevada, Arizona, and California. It is the most important basin in terms of water supply for 25 million people within the basin states and adjoining areas.

Two main mountain ranges, the Rocky Mountains and the Wasatch Mountains, border the east and the west of the basin. The basin contains large variations in topography, climate, soils, and vegetation. Elevations range from 1400 m to about 3700 m. The geologic parent materials provide a wide variety of soils producing vegetation from needle leaf forest complexes to mostly desert shrubs and grasses. In general, the semi-arid region of Lower Colorado River Basin has inhomogeneous and sparse vegetation cover with mixture of vegetation and bare soil patches. Because of its geographic and climatologic characteristics, the Colorado River Basin is particularly vulnerable to severe and sustained drought.

Figure 1 is the σ° image of the LCRB at 10° incidence angle prepared from backscatter observations from multiple orbits. Normalization to 10° is done using a linear relationship between backscatter and incidence angle. Due to orbital geometry of TRMM, 36° N latitude is the upper limit of TRMMPR spatial coverage. The dark area in the east central LCRB is the Coconino forest along the Mogollon ridge and the brighter areas in the image correspond to desert and low vegetation. Corresponding NDVI image is also provided showing predominantly low vegetation cover. Figure 1 also shows the locations of study sites over which the σ° relationship to soil moisture is analyzed. In general, the semi-arid region of LCRB has inhomogeneous vegetation cover with mixture of vegetation and bare soil patches. Since TRMM Ku-band σ° over vegetated area is greatly affected by the canopy scattering we perform our analysis over three different vegetation conditions specified by the NDVI values. In the later text, dense, moderate,

HESSD
6, 6425–6454, 2009

and low vegetation are denoted by *DV*, *MV*, and *LV*, respectively. The NDVI ranges for *LV*, *MV*, and *DV* are 0.2–0.3, 0.3–0.5, and 0.5–0.75, respectively. Sites 1–3 and 4–5 are covered by *DV* and *MV* of Coconino forest, respectively. Locations 8–9 are in the desert north of Coconino forest and are covered with *LV*, primarily, sparse shrubs. Sites 6–7 and 10–12 are locations corresponding to *DV* and *LV*, respectively, in other parts of the basin. Sites 13 and 14 (*LV*) are the locations of gages in the WGEW where top 5 cm soil moisture measurements are used to validate the TRMMPR derived soil moisture.

In order to evaluate consistency of derived soil moisture to the climatic conditions, it is compared with the climate division precipitation data. Climate divisions are regions with relatively homogeneous large-scale climate patterns. National Climate Data Center has used boundaries of US counties, river basins, and major crop areas along with the regional climate statistics to divide US region into climate divisions. These divisions are used as a guide for local analyses and forecasting; and large-scale climate pattern analysis (Guttman and Quayle, 1996). Sites 1–3 (*DV*), 4–5 (*MV*) and 8–9 (*LV*) are in climate division 7 of the state of Arizona and are used for this comparison.

2.2 TRMM Precipitation Radar

TRMM has proved to be a milestone in advancing the understanding of global rain in relation to the hydrologic cycle and climate. The TRMMPR, primarily designed to estimate vertical profile of rain from the path integrated attenuation of the radar pulse, also provides surface σ° measurements (Kummerow et al., 1998; Kozu et al., 2001). These σ° measurements have been used to study vegetation (Stephen and Long, 2002; Satake and Hanado, 2004), deserts (Stephen and Long, 2005), and ocean winds (Li et al., 2004). TRMMPR provides Ku-band HH polarization σ° measurements. Earlier studies on TRMMPR σ° have shown it to be sensitive to the surface soil moisture (Seto et al., 2003; Narayan et al., 2006). This study is the first attempt in a systematic spatial estimation of soil moisture from TRMMPR backscatter data.

TRMMPR σ° measurements are made at θ range of 0°–17°. σ° measurements for

θ less than 3° have high noise. Each TRMMPR measurement record provides a rain flag indicating the precipitation condition for its σ° value. σ° corrupted by rain provides uncertain information about the land surface and thus TRMMPR σ° is cleaned to improve its quality by removing the rain contaminated and near-nadir high noise measurements. TRMMPR measurements are available at four azimuth angles (from ascending and descending passes and cross track scanning towards both sides of satellite path). σ° azimuth modulation is primarily caused by the topography (surface slope). The mean σ° variation due to azimuth angle over LCRB is generally less than 2 dB except along the Mogollon ridge where the surface slope has higher variability. For majority of this area, the azimuth angle dependence is negligible.

TRMMPR σ° observations have a ground resolution of 4.4 km which is reasonably large to include large fractions of bare soil in the arid regions. Thus, in such areas σ° θ dependence is primarily affected by the surface roughness. Large bare soil patches in the TRMMPR footprint significantly influence the backscatter measurements thus introducing strong soil moisture signal in the σ° observations.

2.3 Normalized Difference Vegetation Index

Normalized Difference Vegetation Index is normalized difference of infrared band and red band reflectance and is useful for monitoring vegetation (Tucker, 1979). NDVI has been extensively used to assess ground vegetated land cover. This index benefits from the difference of reflectance of red and near infrared frequencies, which increases with the vegetation density. NDVI is defined as

$$\text{NDVI} = \frac{\text{NIR} - \text{RED}}{\text{NIR} + \text{RED}}$$

where NIR and RED are the near infrared band and red band reflectance, respectively. The normalization results in NDVI values ranging between −1 and 1 where values less than 0 represent bare soil and 1 represents dense vegetation. We use NDVI data prepared from AVHRR that is available in the form of 7-day composite images at

HESSD
6, 6425–6454, 2009

a 1 km ground resolution at the USGS earth explorer website (http://edcsns17.cr.usgs.gov/EarthExplorer/).

2.4 Variable Infiltration Capacity model

VIC is a macro-scale water and energy balance model that uses meteorological, soil, and vegetation data to estimate gridded surface and subsurface runoff (Liang et al., 1994). In this research, we develop VIC model for the LCRB (Tang, 2007). The meteorological data applied to the model includes gridded daily precipitation, minimum and maximum air temperature, and wind speed. We use the gridded meteorological data at 1/8° resolution, prepared by Surface Water Modeling group at the University of Washington (http://www.hydro.washington.edu/Lettenmaier/Data/gridded/). The development of this data is described in (Maurer et al., 2002). The soil data includes field capacity, wilting point, saturated hydraulic conductivity, soil type, and porosity and are obtained from the State Soil Geographic Database maintained by the Earth System Science Center, Pennsylvania. United States Geological Survey (USGS) 30 arc-second digital elevation model is used as a reference for the soil layer depth (Abdulla et al., 1996). The vegetation data is the land composition at each grid cell and constitutes 14 classes. This data is available as University of Maryland 1 km Global Land Cover product and is used to prepare the land cover map. VIC model is forced by gridded precipitation, temperature, wind series, landcover type, and soil properties; and calculates the moisture fluxes for each grid cell. The soil moisture is computed for three soil layers, i.e., 0–10 cm, 10–40 cm, and 40–140 cm. VIC simulated soil moisture has been used for drought analysis (Sheffield et al., 2004) and related to the oceanic-atmospheric patterns (Tang, 2007). We relate water content of the top 10 cm soil layer to the TRMMPR σ° observations. Despite the lack of TRMM coverage in northwest part of basin, the overlap with VIC estimated soil moisture map is sufficient to perform this analysis.

HESSD
6, 6425–6454, 2009

3 Research approach and methods

Backscatter depends upon the surface geometrical (landuse/landcover, soil type and condition, vegetation type and state, etc.) and dielectric (moisture content of vegetation and soil) characteristics. Despite the advances in using σ° in mapping various land parameters, soil moisture mapping is still in its early stages of development. It is difficult to decouple the contributions from geometrical and dielectric features. These characteristics modulate the backscatter measured by TRMMPR. σ° has contribution from vegetation canopy and soil, and their water content. At Ku-band, the vegetation canopy contribution is through the scattering of incident pulse by the leaves, branches, and canopy water called the volume scattering. Ku-band wavelength (2.2 cm) is of the order of small plant leaf sizes. Generally, plant leaves attenuate the power and this attenuation increases with increase in canopy moisture, thus poses difficulty in retrieving soil moisture characteristics from TRMMPR backscatter. Nevertheless, in arid regions where the vegetation is sparse and has large patches of intervening bare soil, Ku-band backscatter is directly affected by the soil moisture. In most of LCRB, the vegetation is non-homogenous and discontinuous resulting in frequent patches of bare soil and low vegetation areas. This contributes to higher dependence of HH-pol Ku-band backscatter on the soil surface conditions i.e., soil type, roughness, and moisture. The relative contribution of soil and vegetation scattering depends upon the vegetation cover and is reflected in the slope of the σ° θ-response. The relationship between σ° and θ is non-linear over the whole range of angles but is approximately linear within 3°–15° incidence angle range.

3.1 Backscatter model

Backscatter θ-response varies with vegetation density and soil moisture. In order to understand the coupled dependence of vegetation and soil moisture, this section presents the analysis of σ° θ-response over three vegetation covers (*DV*, *MV*, and *LV*) and three soil moisture conditions (daily averages: 15–16%, 19–21%, and 24–26%) (see Fig. 2).

HESSD
6, 6425–6454, 2009

In Fig. 2 plots, each symbol point is an individual backscatter measurement at a certain incidence angle. Figure 2a, b, and c correspond to σ° vs. θ plots under three different soil moisture conditions. In each plot, data is shown by different symbols for three vegetation densities. Straight lines are the linear fits to each data set. The analysis of these plots reveals that soil moisture and vegetation modulate the TRMMPR σ° θ-response. In general, an increase in soil moisture increases σ° as well as the slope of σ° θ-response. Vegetation density has the reverse affect on TRMMPR near-nadir backscatter, i.e., as the vegetation density increases, σ° decreases and slope of its θ-response becomes shallower. Based on this analysis, we propose a coupled σ° model given by

$$\begin{aligned}\sigma^\circ(\theta, m_s, \mathrm{NDVI}) = {} & A + B(\theta - \theta_{\mathrm{ref}}) \\ & + C(\theta - \theta_{\mathrm{ref}})(m_s - \mu_s) + D(m_s - \mu_s) \\ & + N(\mathrm{NDVI} - \mu_{\mathrm{ndvi}}) + e. \end{aligned} \quad (1)$$

In this model, the mean annual normalized backscatter A (dB) is modulated by the incidence angle dependence B (dB/$^\circ$), soil moisture dependence D (dB/%), coupled incidence angle and soil moisture dependence C (dB/$^\circ$/%), and NDVI dependence N (dB). θ_{ref} is the reference angle of backscatter incidence angle normalization and chosen as 10° (Ulaby et al., 1982). μ_s (%) and μ_{ndvi} are the annual averages of soil moisture and NDVI, respectively. e is the modeling error. The model takes into account θ, NDVI, and m_s dependence and provides parameters to capture backscatter response to these variables.

The proposed model is applied to the data over the arid lands of LCRB using Least Squared Error Estimation (LSEE) approach. Firstly, the model performance is tested for the selected sites representing the three vegetation densities (*DV*, *MV*, and *LV*). Secondly, the model is applied to all grid cells in the region to retrieve the spatial soil moisture maps. In both model applications, the model calibration is done using 1998 data where the values of model parameters are estimated individually for each point of interest. Later, the estimated model parameter values are used to compute the soil

moisture during 1999.

In order to understand the modeled backscatter dependence on soil moisture, it is necessary that the soil moisture data at desired spatial and temporal scales be available. We use top 10 cm layer VIC soil moisture data to calibrate and validate the proposed backscatter model. The model is also tested for the ground measurements in WGEW.

VIC simulated soil moisture is available at $1/8^{\circ} \times 1/8^{\circ}$ grid (approximately 12×12 km grid in LCRB region). In this study, point based and spatial analyses of the proposed model are performed at the VIC spatial resolution, i.e., the TRMMPR σ° measurements within a given 12×12 km VIC cell are used in model-parameter and soil moisture estimation. Due to coarser combined incidence angle and temporal sampling of σ°, a ten day moving window with five day steps is used for σ° model inversion and m_s averaging. NDVI data (1 km resolution) is also smoothed to match the VIC resolution.

3.2 Backscatter model calibration

The model is applied to the three study sites with *DV*, *MV*, and *LV* vegetation covers using LSEE approach and the surface fits at μ_{ndvi} are shown in Fig. 3. The corresponding model parameters are listed in Table 1. The model parameters over all the listed sites are computed using the 1998 soil water content and NDVI data.

Table 1 data reveals that *A* decreases whereas *B* increases with vegetation density. It is noted that *B* values are generally negative and thus an increase in *B* implies reduction in the physical slope of the line. *B* depends upon the relative contribution of surface and volume scattering. Under dense vegetation conditions, *B* can have positive values because σ° at near-nadir incidence angles over such land cover is lower due to higher attenuation from leaves. With an increase in the incidence angle higher backscattering is caused due to the predominant leaf orientations. This effect reduces with vegetation density. The parameters *C* and *D* correspond to the sensitivity to water content. The magnitudes of *C* and *D* reduce with increase in vegetation cover. Low *B* values reflect low vegetation and more bare soil, thus, for low *B* values, *C* and *D* are

the σ° sensitivities to water content of soil. N is the change in σ° per unit change in NDVI.

The model has been also studied without incorporating and NDVI data (dropping the 5th term on the right hand side of Eq. (1). We note that adding NDVI dependence slightly improves the model performance. The reason being that the vegetation dependence of the model is also incorporated in the other parameters (especially captured in the values of A and B).

The results over selected study sites show the potential of Ku-band backscatter measurements to map soil moisture over the arid regions. In order to evaluate the applicability of this approach at basin scale, we compute the model parameters at each grid cell in LCRB. The VIC m_s and NDVI data at each grid cell in LCRB along with corresponding TRMMPR σ° measurement during 1998 are used to compute the model parameters at each grid cell. It is noted that the model described in Eq. (1) is applied individually to each grid cell and thus results in separate model parameters for at each grid cell. The spatial maps of the model parameters are shown in Fig. 4 along with root mean square error of the model fit at each point. The error is high along the Mogollon ridge due to the highly varying topography. The backscatter dependence on NDVI (N) and average NDVI values during 1998 is also shown. Since the computation is grid based, the output is a spatial distribution of the model parameters.

The dense vegetation has lowest A due to high attenuation of Ku-band waves by the leaves in the canopy. The bright spot in the middle of the A image is from the city of Phoenix, Arizona. A increases with reduction in vegetation density towards northeast and southwest. B values are also consistent with the vegetation density and lows occur over the desert region where surface scattering dominates. The dense vegetation has the highest mean annual soil moisture μ_s that reduces over the shrubs and desert area in the northeast and southwest. D measures the backscatter sensitivity to soil moisture which reduces in the areas of higher vegetation density. It has low values over the dense vegetation and high values over the desert. In the desert area, this sensitivity is also dependent upon the soil type and existence of rocky surfaces. This is evident in

the image where low values of D occur in the desert region. C is a measure of variability in the sensitivity of soil moisture to backscatter. Even though it is linked to the relative contribution of surface and volume scattering, it is related to vegetation density and moisture. In the image, the very low values occur over the non-vegetated areas with high surface roughness. In these areas, increase in moisture will significantly alter the σ° θ-response from soil-surface-like-response to dense-vegetation-like-response. μ_{ndvi} is the average annual NDVI in the region whereas N quantifies the effect of annual change in the NDVI on σ° measurements.

4 Results and discussion

Calibrated models described in the previous section are used to compute the soil moisture during 1999. The computed model parameters from the 1998 data listed in Table 1 are used to derive soil water content from TRMMPR σ° data during the later years by reordering of Eq. (1), i.e.,

$$m_s = \mu_s + \frac{\sigma^\circ - A - B(\theta - \theta_{\text{ref}}) - N(\text{NDVI} - \mu_{\text{ndvi}})}{C(\theta - \theta_{\text{ref}}) + D}. \quad (2)$$

Figure 5a compares the time series of TRMMPR derived and VIC estimated soil moisture during 1999 at the study site 12. The temporal variation of the soil water content derived by the model is in agreement with the VIC estimates. The model performance deteriorates under extreme dry and wet conditions. Figure 5b plots the regression lines for the study sites 1 (*DV*), 4 (*MV*), and 12 (*LV*) where the R is 0.57, 0.66, and 0.78, respectively. The correlation reduces with vegetation density.

Vegetation increases the volume scattering thus decreasing the slope of σ° θ-response line. It depends upon the characteristics of vegetation layer such as leaf area index and canopy water content. Dense vegetation attenuates the electromagnetic energy and reduces the sensitivity to the underlying soil characteristics. This effect is more severe under wet canopy condition. The Ku-band has higher attenuation

HESSD
6, 6425–6454, 2009

by the canopy. This significantly reduces the σ° values at low incidence angles thus reducing A and increasing the value of B.

The water content increases the σ° and this effect is higher at low incidence angles. It results in an increase in A and decrease in B. The σ° sensitivity to soil moisture depends on the vegetation cover density and vegetation water content. Over dense vegetation the soil moisture signal is over-shadowed by vegetation backscatter and difficult to detect. With decrease in vegetation density the contribution from the soil increases thus raising the sensitivity to the soil water content. The presence of water in the vegetation reduces the penetration through canopy thus reducing the sensitivity to soil water content. In this case, the σ° is primarily reflecting the canopy water content. Under very dry conditions, the soil and vegetation have low dielectric constant (Ulaby et al., 1982). Thus, TRMMPR backscatter has dominant effect of the surface geometry.

In a similar manner, the model is also used to estimate the soil water content at study site 14 in the WGEW during 1999–2006. In this case, the results are compared to gage measurements plotted in Fig. 6a. Gage measurements during most of the year 2002 are not available. Nevertheless, the model captures quite well the temporal behavior of measured soil moisture. As seen earlier, the derived soil water content accuracy reduces under extreme dry and wet conditions. The corresponding regression line and correlation are shown in Fig. 6b. The model accuracy reduces with time since the model calibration is performed using 1998 data.

The temporal variation of soil moisture is linked to the precipitation illustrated in Fig. 7a. The time series corresponds to the climate division 7 of Arizona where monthly averages of derived soil water content are computed using the data from study sites 1–5 and 8–9 (these sites fall in this climate division). The derived soil water content provides a temporal behavior during 1999–2006 that is similar to the monthly averages of the measured precipitation data with a correlation of 0.76 (see Fig. 7b).

The analysis of derived soil water content to measured soil moisture and precipitation data confirms the potential of TRMMPR σ° data for soil moisture retrieval in the LCRB. The proposed model captures the general temporal variation of the soil mois-

HESSD
6, 6425–6454, 2009

ture. The model is able to derived soil water content over different vegetation covers in the arid region of LCRB where the sensitivity to soil moisture reduces with increase in vegetation cover.

Using the same approach we estimate the spatial soil moisture maps. The spatial maps of the computed model parameters (Fig. 4) are used to derive the spatial maps of soil water content from σ° measurements during May (dry period) and August (wet period) of 1999. Figure 8 compares the maps of model derived and VIC soil water content over the TRMM coverage of LCRB. The maps are compared during dry and wet times of the year 1999. As seen earlier in the analysis over selected study sites, the model performs better during wet season. In wet season (August), the spatial distribution of derived soil water content is similar to the VIC estimates with R=0.76. The dissimilarities correspond to very dry and very wet areas of the basin. Although the correlation during dry season is lower (0.67), a general similarity in the spatial distributions is evident.

We approached this study with a goal to develop a simple model that can explain relationship between backscatter and soil moisture. The proposed model is shown to provide good soil moisture estimates in LCRB and would perform well in other similar (arid and semi-arid) settings. It is difficult to decouple the impact of all surface characteristic on the backscatter measurements. The complex dependence of microwave scattering on surface roughness, soil moisture, and vegetation is simplified in a linear model that works well over mixed patches of bare soil and vegetation (typical of arid and semi-arid land surfaces) in the radar footprint. Application of the model over large basin provides good estimates of soil moisture without accounting for surface roughness effects. At this scale the surface roughness effect is captured in the incidence angle dependence of TRMMPR backscatter. Though desirable, explicit incorporation of surface roughness into the model would complicate the model without, perhaps, significantly improving the results. In regions with dense vegetation, the model performance deteriorates (as seen by reduced correlation). In such regions, the soil moisture signal at Ku-band is primarily originating from the vegetation canopy. The model

HESSD

6, 6425–6454, 2009

performance also deteriorates under high soil moisture conditions especially if such conditions persist over several days.

5 Conclusions

Soil moisture is an important parameter to understand the hydrologic cycle. The soil moisture measured data is scarce and alternative approaches are needed for its spatial mapping. Radar backscatter over land depends upon the soil moisture and vegetation characteristics of the land surface. In case of arid regions, such as LCRB, due to sparse vegetation, backscatter primarily depends on the soil moisture characteristics. A new technique that relates σ° response to NDVI and soil moisture data in arid regions is presented. TRMMPR σ° is modeled as a function of incidence angle, NDVI, and soil water content. The model calibration is performed using the known soil moisture data from VIC estimates and gage measurements; and NDVI data during 1998. The model is tested over selected study sites in LCRB with varying vegetation cover. The model parameters reflect the surface characteristics and the σ° sensitivity to soil water content and NDVI. The model is used to derive the soil water content during 1999–2006 and provides results consistent with the VIC estimated and in-situ measurements. The results are temporally consistent with the time series of measured precipitation data. The spatial maps of the soil water content are derived for dry and wet periods during 1999 and are consistent with the VIC estimates. The spatial coherence of these maps confirms the ability of TRMMPR to map soil moisture.

This research provides an approach to use spaceborne backscatter data for soil moisture retrieval. The model presented in the research is point-based model and provides gridded model parameters. It is a generic model with parameters that depend on surface type. The proposed model is simple yet reasonably accurate for quick retrieval of large scale soil moisture maps from backscatter data. The model inherits its spatial resolution from the input data and captures the average large scale dependence of backscatter on soil moisture and vegetation. Thus, it is suitable for studies of large

scale watersheds. The devised approach presents an alternative to the usual unavailability of in-situ soil moisture measurements. Due to coarse resolution of TRMMPR, the estimated soil moisture can be used in large scale hydrological and meteorological models. Finer scales (<4 km) may require downscaling.

The accuracy of this model reduces under extreme dry and wet surface conditions. Under very dry condition, σ° is primarily a function of the surface geometry and thus does not reflect the soil water content resulting in the erroneous estimates. During very wet period, soil saturation is the main source of errors in the estimates.

Acknowledgements. The work was partly funded by NOAA Award # NA07OAR4310324. Soil Moisture data from Walnut Gulch Experimental Watershed is provided by the USDA-ARS Southwest Watershed Research Center.

References

Abdulla, F. A., Lettenmaier, D. P., Wood, E. F., and Smith, J. A.: Application of a macroscale hydrological model to estimate the water balance of the Arkansas Red river, J. Geophys. Res.-Atmos., 101, 7449–7459, 1996. 6433

Barrett, B. W., Dwyer, E., and Whelan, P.: Soil moisture retrieval from active spaceborne microwave observations: An evaluation of current techniques, Remote Sens., 1, 210–242, doi:10.3390/rs1030210, 2009. 6427

Baup, F., Mougin, E., de Rosnay, P., Timouk, F., and Chênerie, I.: Surface soil moisture estimation over the AMMA Sahelian site in Mali using ENVISAT/ASAR data, Remote Sens. Environ., 109(4), 473–481, 2007. 6427

Behari, J.: Microwave Dielectric Behavior of Wet Soils, Springer, New York, USA, 2005. 6427

Bindlish, R., Jackson, T. J., Wood, E., Gao, H., Starks, P., Bosch, D., and Lakshmi, V.: Soil moisture estimates from TRMM Microwave Imager observations over the Southern United States, Remote Sens. Environ., 85(4), 507–515, 2003. 6428

Cosh, M. H., Jackson, T. J., Moran, S., and Bindlish, R.: Temporal persistence and stability of surface soil moisture in a semi-arid watershed, Remote Sens. Environ., 112, 304–313, 2008. 6427

Das, N. N., Mohanty, B. P., Cosh, M. H., and Jackson, T. J.: Modeling and assimilation of root zone soil moisture using remote sensing observations in Walnut Gulch Watershed during SMEX04, Remote Sens. Environ., 112, 415–429, 2008. 6428

ESA Study Report: Soil moisture retrieval by a future space-borne Earth Observation Mission, ESA Study Report 14662/00/NL, 2004. 6427

Fung, A. K.: Microwave Scattering and Emission Models and Their Applications, Artech House, Inc., Boston, Massachusetts, 1994. 6428

Guttman, N. B. and Quayle, R.: A historical perspective of U.S. climate divisions, B. Am. Meteorol. Soc., 77(2), 293–303, 1996. 6431

Kozu, T., Kawanishi, T., Kuroiwa, H., Kojima, M., Oikawa, K., Kumagai, H., Okamoto, K., Okumura, M., Nakatsuka, H., and Nishikawa, K.: Development of Precipitation Radar onboard the Tropical Rainfall Measuring Mission (TRMM) satellite, IEEE T. Geosci. Remote, 39(1), 102–116, 2001. 6428, 6431

Kummerow, C., Barnes, W., Kozu, T., Shiue, J., and Simpson, J.: The Tropical Rainfall Measuring Mission (TRMM) sensor package, J. Atmos. Ocean. Tech., 15, 808–816, 1998. 6428, 6431

Li, L., Im, E., Connor, L. N., and Chang, P. S.: Retrieving ocean surface wind speed from the TRMM Precipitation Radar, IEEE T. Geosci. Remote, 42(6), 1271–1282, 2004. 6431

Liang, X., Lettenmaier, D. P., Wood, E. F., and Burges, S. J.: A simple hydrologically based model of land-surface water and energy fluxes for general-circulation models, J. Geophys. Res.-Atmos., 99(D7), 14415–14428, 1994. 6429, 6433

Magagi, R. D. and Kerr, Y. H.: Retrieval of soil moisture and vegetation characteristics by use of ERS-1 Scatterometer over arid and semi-arid areas, J. Hydrol., 188–189, 361–384, 1997. 6427

Moran, M. S., Peters-Lidrad, C. D., Watts, J. M., and McElroy, S.: Estimating soil moisture at the watershed scale with satellite-based radar and land surface models, Can. J. Remote Sens., 30(5), 805–826, 2004. 6427

Maurer, E. P., Wood, A. W., Adam, J. C., Lettenmaier, D. P., and Nijssen, B.: A long-term hydrologically based dataset of land surface fluxes and states for the conterminous United States, J. Climate, 15, 3237–3251, 2002. 6433

Narayan, U., Lakshmi, V., and Jackson, T.: A simple algorithm for spatial disaggregation of radiometer derived soil moisture using higher resolution radar observations, IEEE T. Geosci. Remote, 44(6), 1545–1554, 2006. 6428, 6431

Njoku, E. G., Jackson, T. J., Lakshmi, V., Chan, T. K., and Nghiem, S. V.: Soil moisture retrieval from AMSR-E, IEEE T. Geosci. Remote, 41(2), 215–229, 2003. 6427

Paloscia, S., Macelloni, G., Santi, E., and Koike, T.: A multifrequency algorithm for the retrieval of soil moisture on a large scale using microwave data from SMMR and SSM/I satellites, IEEE T. Geosci. Remote, 39(8), 1655–1661, 2001. 6428

Pulliainen, J. T., Manninen, T., and Hallikainen, M.: Application of ERS-1 Wind Scatterometer data to soil frost and soil moisture monitoring in Boreal forest zone, IEEE T. Geosci. Remote, 36(3), 849–863, 1998. 6427

Rahman, M. M., Moran, M. S., Thoma, D. P., Bryant, R., Collins, C. D. H., Jackson, T., Orr, B. J., and Tischler, M.: Mapping surface roughness and soil moisture using multi-angle radar imagery without ancillary data, Remote Sens. Environ., 112, 391–402, 2008. 6428

Satake, M. and Hanado, H.: Diurnal change of Amazon rain forest σ° observed by Ku-band spaceborne radar, IEEE T. Geosci. Remote, 42(6), 1127–1134, 2004. 6431

Schmugge, T. J.: Remote sensing of soil moisture: Recent advances, IEEE T. Geosci. Remote, GE-21(3), 336–344, 1983. 6427

Seto, S., Oki, T., and Musiake, K.: Surface soil moisture estimation by TRMM/PR and TMI, in: Proceedings of International Geoscience and Remote Sensing Symposium, vol. III, 1960–1962, IEEE, 2003. 6428, 6431

Sheffield, J., Goteti, G., Wen, F., and Wood, E. F.: A simulated soil moisture based drought analysis for the United States, J. Geophys. Res., 109, D24108, doi:10.1029/2004JD005182, 2004. 6427, 6433

Shi, J., Wang, J., Hsu, A. Y., O'Neill, P. E., and Engman, E. T.: Estimation of bare surface soil moisture and surface roughness parameter using L-band SAR image data, IEEE T. Geosci. Remote, 35(5), 1254–1266, 1997. 6428

Stephen, H., and Long, D. G.: Multi-spectral analysis of the Amazon basin using Seawinds, ERS, NASA, Seasat Scatterometer, TRMM-PR and SSM/I, in: Proceedings of Intl. Geosc. and Rem. Sens. Symp., Toronto, Canada, vol. 5, 2808–2810, 2002. 6431

Stephen, H. and Long, D. G.: Microwave backscatter modeling of erg surfaces in the Sahara desert, IEEE T. Geosci. Remote, 43(2), 238–247, 2005. 6431

Tang, C.: Soil moisture and hydrological drought in the Upper Colorado River basin, Ph.D. thesis, University of Nevada, Las Vegas, NV, 2007. 6429, 6433

Tucker, C. J.: Red and photographic infrared linear combinations for monitoring vegetation, Remote Sens. Environ., 8, 127–150, 1979. 6432

Ulaby, F., Moore, R., and Fung, A.: Microwave Remote Sensing: Active and Passive, vol. 3, Artech House, Inc., Norwood, Massachusetts, 1982. 6428, 6435, 6439
Wagner, W., Blöschl, D., Pampaloni, P., Calvet, J.-C., Bizzarri, B., Wigneron, J.-P., and Kerr, Y.: Operational readiness of microwave remote sensing of soil moisture for hydrologic applications, Nord. Hydrol., 38(1), 1–20, 2007. 6427
Wen, J., Su, Z., and Ma, Y.: Determination of land surface temperature and soil moisture from Tropical Rainfall Measuring Mission/Microwave Imager remote sensing data, J. Geophys. Res., 108(D2), 805–826, 2003. 6428
Woodhouse, I. H. and Hoekman, D. H.: A model-based determination of soil moisture trends in spain with ERS-scatterometer, IEEE T. Geosci. Remote, 38(4), 1783–1793, 2000. 6427

Table 1. List of model parameters of Eq. (1) using VIC soil water content for three vegetation densities.

	Vegetation Density		
Parameter	Low	Moderate	Dense
A (dB)	−4.88	−7.25	−8.77
D (dB/%)	0.29	0.27	0.08
B (dB/°)	−0.52	−0.42	0.17
C (dB/°/%)	−0.023	−0.017	−0.004
N (dB)	6.84	2.16	−3.64
μ_{ndvi}	0.27	0.5	0.67
μ_s	18.77	19.32	24.27

HESSD
6, 6425–6454, 2009

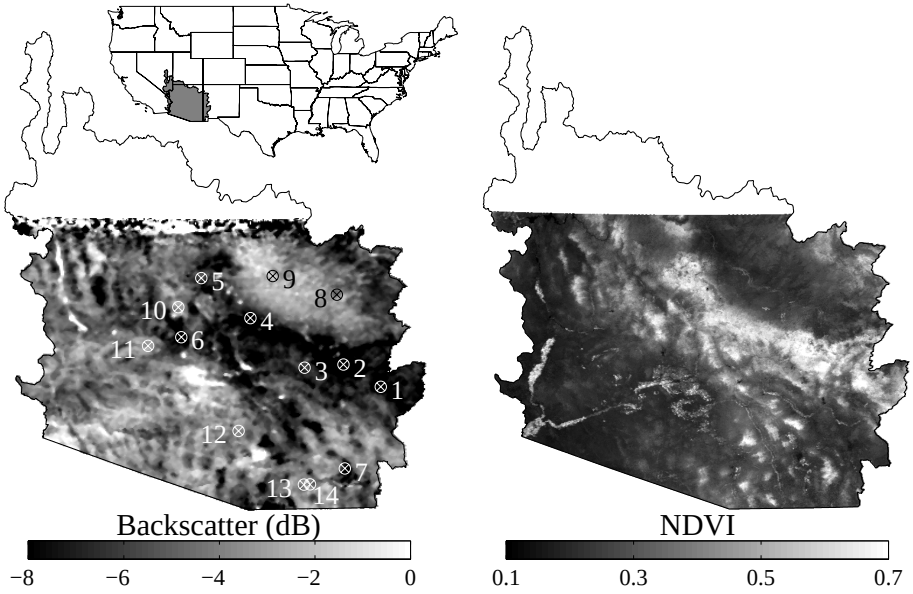

Fig. 1. Backscatter map of the Lower Colorado River Basin showing locations of study sites used in this research. Basins geographical position in the US is also shown and bounded within 31°–40° N latitudes and 107°–116° W longitudes. Northwest basin area is not covered by TRMM satellite. (Right) Corresponding vegetation (NDVI) map of the basin.

HESSD
6, 6425–6454, 2009

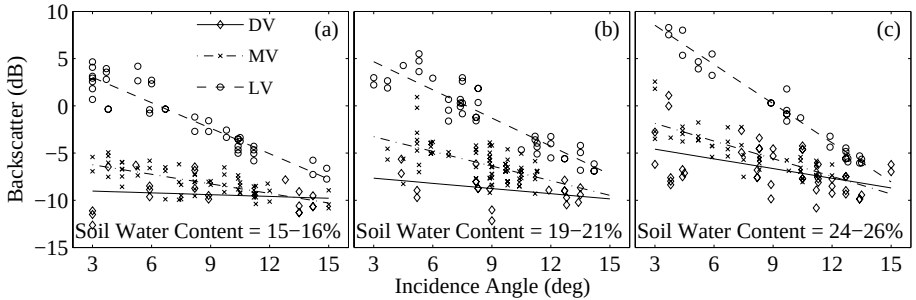

Fig. 2. Backscatter incidence angle dependence for three vegetation densities (dense, moderate, and low) and three soil water content values, i.e., **(a)** 15–16%, **(b)** 19–21%, and **(c)** 24–26%.

HESSD
6, 6425–6454, 2009

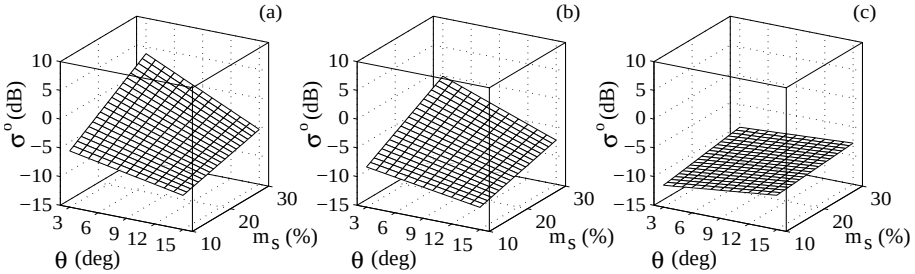

Fig. 3. Surface fit to backscatter (σ°) dependence on incidence angle (θ) and soil water content (m_s) (Eq. 1) over **(a)** low, **(b)** moderate, and **(c)** dense vegetation.

HESSD
6, 6425–6454, 2009

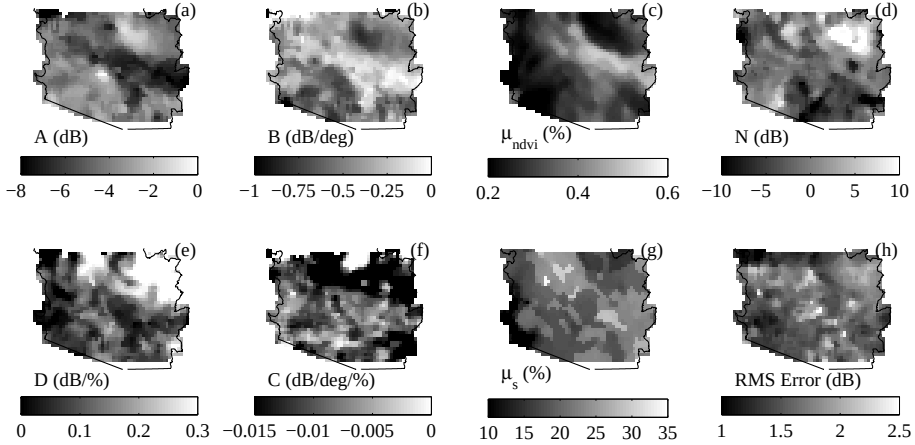

Fig. 4. Images of model parameters **(a)** A, **(b)** B, **(c)** μ_{ndvi}, **(d)** N, **(e)** D, **(f)** C, and **(g)** μ_s. **(h)** Root Mean Square (RMS) error image.

HESSD
6, 6425–6454, 2009

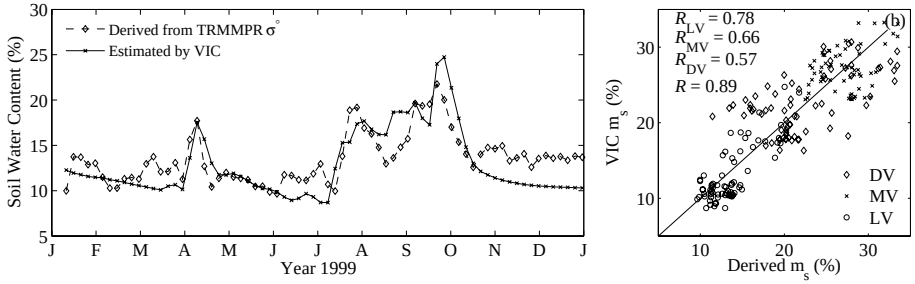

Fig. 5. **(a)** Comparison of 1999 temporal variation of VIC and TRMMPR derived soil water content over low vegetation area. **(b)** Regression analysis over three study sites, i.e., *DV*, *MV*, and *LV*.

HESSD
6, 6425–6454, 2009

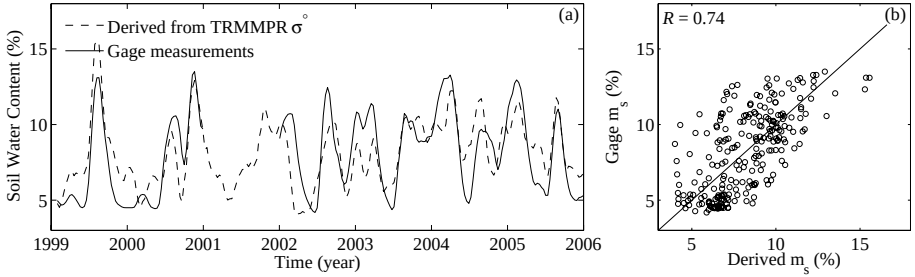

Fig. 6. **(a)** Comparison of TRMMPR derived and gage soil water content in Walnut Gulch Experimental Watershed. **(b)** Data scatter plot and correlation.

HESSD
6, 6425–6454, 2009

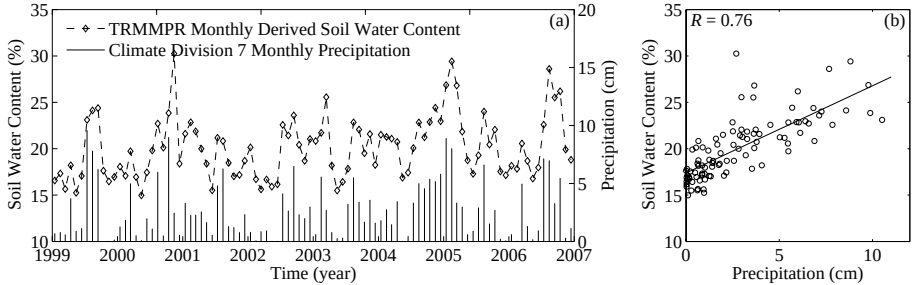

Fig. 7. (a) Comparison of TRMMPR derived soil water content and monthly average precipitation in the climate division 7 of Arizona. **(b)** Regression line of datasets.

HESSD
6, 6425–6454, 2009

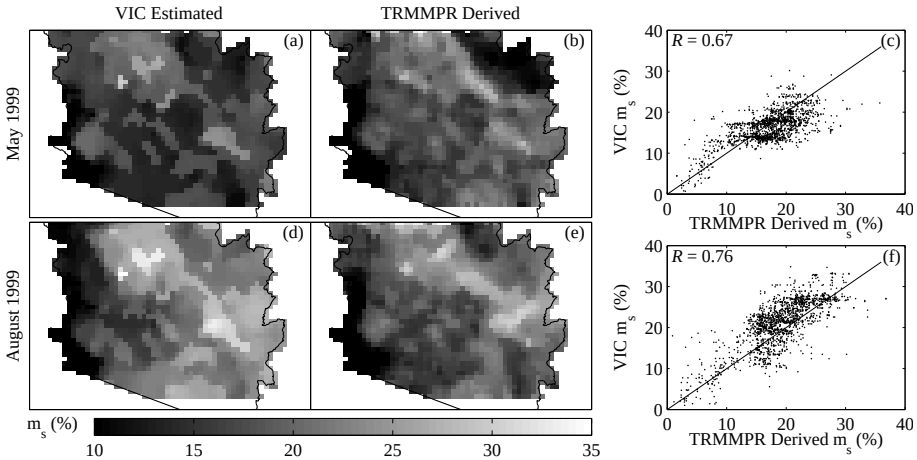

Fig. 8. Comparison of VIC (left column) and TRMMPR derived (center column) soil moisture images during dry (top row) and wet (bottom row) periods. The corresponding regression lines (right column) are also shown.

HESSD
6, 6425–6454, 2009